Nuclear Engineering and Design 310 (2016) 470–483

Contents lists available at ScienceDirect

Nuclear Engineering and Design

journal homepage: www.elsevier.com/locate/nucengdes

Theoretical assessment of particle generation from sodium pool fires

M. Garcia [a,*], L.E. Herranz [a], M.P. Kissane [b]

[a] CIEMAT, Unit of Nuclear Safety Research, Av. Complutense, 40, 28040 Madrid, Spain
[b] Nuclear Safety Technology and Regulation Division, OECD Nuclear Energy Agency (NEA), 46 quai Alphonse Le Gallo, 92100 Boulogne-Billancourt, France

HIGHLIGHTS

- Development of particle generation model for sodium-oxides aerosol formation.
- Development of partially validated numerical simulations to build up maps of saturation ratio.
- Nucleation of supersaturated vapours as relevant source of aerosols over sodium pools.
- Prediction of high concentrations of primary particles in the combustion zone.

ARTICLE INFO

Article history:
Received 15 June 2016
Received in revised form 19 October 2016
Accepted 22 October 2016
Available online 31 October 2016

Keywords:
Particle generation rate
Primary particle size
In-containment SFRs
Numerical simulation
Sodium pool fire

ABSTRACT

Potential sodium discharge in the containment during postulated Beyond Design Basis Accidents (BDBAs) in Sodium-cooled Fast Reactors (SFRs) would have major consequences for accident development in terms of energetics and source term. In the containment, sodium vaporization and subsequent oxidation would result in supersaturated oxide vapours that would undergo rapid nucleation creating toxic aerosols. Therefore, modelling this vapour nucleation is essential to proper source term assessment in SFRs. In the frame of the EU-JASMIN project, a particle generation model to calculate the particle generation rate and their primary size during an in-containment sodium pool fire has been developed. Based on a suite of individual models for sodium vaporization, oxygen natural circulation (3D modelling), sodium-oxygen chemical reactions, sodium-oxides-vapour nucleation and condensation, its consistency has been partially validated by comparing with available experimental data. As an outcome, large temperature and vapour concentration gradients set over the sodium pool have been found which result in large particle concentrations in the close vicinity of the pool.

© 2016 Elsevier B.V. All rights reserved.

1. Introduction

Generation IV (Gen. IV) designs are striving to reach the highest safety standards ever applied to Nuclear Power Plants (NPPs). Accidents with significant fuel damage (i.e., severe accidents) are being considered in the design phase so that they can be inherently avoided or prevented and/or mitigated by passive design features or by ad-hoc engineering safeguards with elimination of the need for offsite emergency response (GIF, 2002). This enlargement of design scope with respect to Gen. II and Gen. III reactors is a challenge for all the technologies involved in the systems chosen for Gen. IV since accident scenarios involve complex phenomena that have to be taken into account when demonstrating reactor safety. Sodium-cooled Fast Reactor (SFR) technology is more mature than other Gen. IV designs since several SFR reactors have been operated (i.e., BN-600, Phénix, Joyo, FBTR, etc.) and, as a result, the experience that has been gained currently amounts to >400 operational years. Nonetheless, in Europe, if France chooses to pursue SFR development, the new technologies to be used as well as higher safety standards to be put in place will require the construction of an "industrial demonstrator", called ASTRID, which might start operation around 2030 (CEA, 2015).

In SFR systems, sodium (Na) is used as a coolant due to its excellent properties. Its high thermal conductivity and low viscosity make it a good thermal-energy transport fluid with a broad temperature interval as a liquid (370–1156 K at atmospheric pressure) allowing its use as coolant in low pressure conditions close to the ambient conditions. In addition, it is also suitable for the fast-neutron economy since its absorption and scattering cross sections are very low; finally, its compatibility with structural materials is quite good (in comparison with heavy liquid metals like lead, lead-bismuth eutectic, ...). However, despite all these advantages,

* Corresponding author.
E-mail addresses: monica.gmartin@ciemat.es (M. Garcia), luisen.herranz@ciemat.es (L.E. Herranz), Martin.KISSANE@oecd.org (M.P. Kissane).

http://dx.doi.org/10.1016/j.nucengdes.2016.10.024
0029-5493/© 2016 Elsevier B.V. All rights reserved.

Na shows a high chemical reactivity with oxygen, and in a less extent water, which entails a fire hazard risk in case of leaks into the containment.

In SFR safety studies the highly-unlikely event of a core disruptive accident must be considered. In accident conditions, core disruption by supercriticality could involve energetic destruction of fuel assemblies. Then, if this is assumed, the interaction between hot fuel and liquid sodium could lead to a vapour explosion which could create a breach in the primary system and contaminated liquid sodium at high temperature would be ejected into the containment. In these conditions, the vaporization of sodium and its possible instantaneous combustion with the oxygen available would result in the generation of supersaturated Na-oxide (Na_xO_y) vapours likely to nucleate and form suspended particles. The aerosols formed could act as a radioactive species carrier; this together with the potential harm associated with the chemical species resulting from the sodium oxides reaction with water vapour present in the atmosphere (sodium hydroxide aerosols) would be responsible to a great extent for the radiological and chemical impact of any potential source term. In addition, if the leak is major, the heat released during the combustion is substantial.

Several sodium fire studies (pool and spray fires) have been carried out since the 1970s, in facilities like PLUTON (Lhiaubet et al., 1990) and JUPITER (Malet et al., 1990) in France, CSTF in the USA (Hilliard et al., 1977, 1979; McCormack et al., 1978 and Souto et al., 1994), FAUNA in Germany (Cherdron and Jordan, 1980, 1983; Cherdron et al., 1985, 1990) or ATF in India (Subramanian and Baskaran, 2007; Subramanian et al., 2009; Baskaran et al., 2011). In all of them, the aim was to understand the sodium burning process and to study the sodium compound aerosols behaviour and their chemical composition. Since then a number of studies have intended to model the whole scenario with relative success.

The pioneering work by Beiriger et al. (1973), who developed a tool mainly focused on fire energetics (the SOFIRE code), was followed by others who made specific hypotheses and approximations. In the SOFIRE model, the formation of a thin vapour layer over the surface of the pool is not considered and the Na-O_2 reactions take place on the pool surface. Through an extensive review of the physico-chemical processes involved in the liquid sodium pool combustion, Newman (1983) established that pool combustion could occur via surface or gas-phase reaction depending on the ignition temperature. Based on this work, Sagae and Suzuoki (1985) developed an analytical combustion model in which sodium vapour diffuses from the pool surface to a flat flame where the Na-O_2 reactions take place. In this model the combustion rate depends on heat and mass transfer of Na and O_2 to the flame (flame sheet approach). The vapour-phase sodium-combustion model has been included in numerous combustion codes as the SPM code by Miyake et al. (1991), SOPA code developed by Lee and Choi (1997) or more recently in multi-dimensional numerical analysis codes such as the SPHINCS code (Yamaguchi and Tajima, 2003a) or AQUA-SF code (Takata et al., 2003).

However, as said above, all these computer codes have mostly focused on energetics and thermal-hydraulics (Murata et al., 1993) so that particle modelling has received much less attention. For example: the SOFIRE code (Beiriger et al., 1973) assumes that all Na_xO_y produced becomes particles of a given size with no consideration of particle formation kinetics or primary-particle size; the CONTAIN-LMR code (Murata et al., 1993) requires the user to fix the initial particle size in the analysis and this becomes the size at which any particle is nucleated.

This paper presents the main features and bases of a Particle Generation (PG) model from sodium pool fires whose main output variables are particle generation rate and size. This consists of a suite of individual models of the following phenomena involved: Na vaporization (diffusion layer approach), O_2 transport by air natural circulation (3D flow pattern modelling), Na-O_2 chemical reactions (instantaneous reactions and energy input) and vapour-to-particle conversion (Na_xO_y vapours nucleation by Classical Nucleation Theory and condensation by kinetic theory of gases). Although direct model validation is not feasible due to the lack of experimental data on Na_xO_y vapour nucleation, a partial model validation of sodium vaporization, air convection and sodium reactions has been carried out against available experimental data.

Consequently, the scope of the presented model is the estimation of the particle generation by homogeneous and heterogeneous nucleation during an in-containment sodium pool fire in the near field of the pool. The main output of the model is the number concentration and size of the primary particles resulting from the Na pool combustion. Therefore, any further consideration of particles growth by agglomeration, chemical reaction with steam and/or other gases (like CO_2) and transport to other regions in the far-field of the pool, are out of the scope of the present paper. Any of these additional phenomena would be essential for a full prediction of in-containment source term behaviour and, as such, they would be encapsulated in specific models in a lumped parameter code addressing SFR severe accidents, in which the present work would be embedded as a particle source into the containment atmosphere.

This work has been mostly carried out in the frame of the 7th Framework Programme of the European Commission via the JASMIN project.

2. Conceptual scenario

Liquid-sodium-pool combustion can proceed via surface reaction or gas-phase reaction depending on the initial pool temperature. Newman (1983) showed that when the pool temperature is lower than the ignition one (623–723 K), surface reaction dominates, forming a grey-purple product close to the sodium surface that acts as a floating layer on the surface of the liquid sodium without any combustion; however, for sodium pool temperatures higher than the ignition one, this grey layer wets or decomposes allowing Na vapour to vaporize. Assuming instantaneous combustion, this would occur in the gas phase in a layer called the flame region located close to the pool; it is in this region where the sodium oxide vapours would form, nucleate and create particle growth.

The gas-phase reaction region is sketched in Fig. 1, in which the Na pool is displayed as a hot flat plate. As observed, the pool nearby can be split into three layers: sodium vapour, right over the pool; a flame region, above and adjacent to the Na layer; and the bulk gas overlying the flame and feeding the flame region with oxygen by natural convection (Miyake et al., 1991; Newman and Payne, 1978; Newman, 1983).

At steady-state burning, the pool does not reach its boiling point but remains close to the commonly found equilibrium pool temperature of 1000–1010 K (Newman and Payne, 1978). On the other side, vapour pressure of sodium is approximately 1 kPa at 800 K and very nearly 20 kPa at 1000 K. In these conditions, sodium readily evaporates and this vapour will be transported by diffusion to the flame region in which Na vapour reacts with the available oxygen forming Na-oxides and making the local temperature rise to 1200–1300 K. Namely, sodium oxidation is sustained by Na diffusion and by O_2 brought to the region by turbulent convective flows in the gas over the pool surface. As sodium vapour supply by evaporation becomes relatively large and chemical reactions are known to be fast, sodium combustion will be governed by Na vapour supply by evaporation and oxygen transport into the reaction region. In the sodium vapour layer, a vertical laminar flux will exist from the sodium pool surface to the flame region,

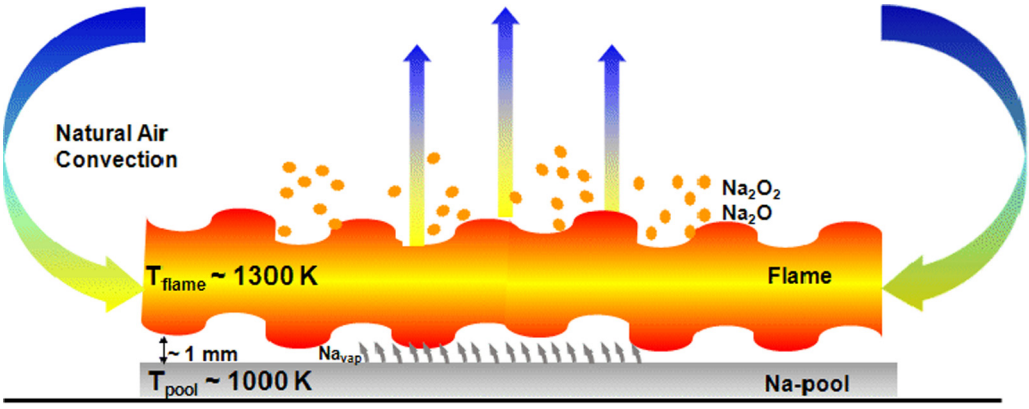

Fig. 1. Hot flat plate approach.

whereas in the flame region, the flow field will become fully turbulent under the natural convection regime for pool diameters >0.1 m (Newman, 1983).

The Na-oxide compounds formed (Na_2O and Na_2O_2) have at the flame temperature vapour pressures well in excess of their saturation pressures, so that molecules cluster by homogeneous nucleation forming very small primary particles. As soon as these first seeds appear, the vapour-phase oxide molecules also condense on the surface of these nucleated particles if vapour pressure is higher than saturation pressure at the particle surface temperature (i.e., heterogeneous nucleation occurs).

3. Global modelling of particle generation

Based on the conceptual physico-chemical scenario described above, global modelling of Particle Generation (PG model) has been developed. As a result, particle generation rate and primary-particle size can be obtained for a sodium pool fire in a SFR containment. In this model, steady-state burning is assumed.

The PG model comprises the individual phenomena involved in the particle generation process during a sodium pool fire, namely: Na vaporization, O_2 natural convection, Na-O_2 chemical reactions and vapour-to-particle conversion of Na oxides. The PG model sequence diagram is shown in Fig. 2. From the sodium pool definition by the pool temperature and the pool diameter, the vaporized Na from the pool surface is obtained through a Sodium Vaporization Model (SVM). Due to the extreme foreseen conditions above the combustion zone (high turbulence is foreseen), a steady 3D Computation Fluid Dynamics (CFD) approach is employed based on the FLUENT code (ANSYS, 2008). In this numerical simulation, the O_2 natural convection and the Na-O_2 chemical reactions are modelled (O_2 Supply Model, O_2SM; Na-O_2 Chemical Model, Na-O_2ChM) for an appropriate estimation of the thermal-hydraulic boundary conditions in the region of interest, i.e., in the close vicinity of the sodium reaction zone. In the Vapour-to-Particle Conversion model (VtPCM), particle generation by homogeneous nucleation and particle growth by condensation are accounted for. As a result, the PG model produces the total number rate of

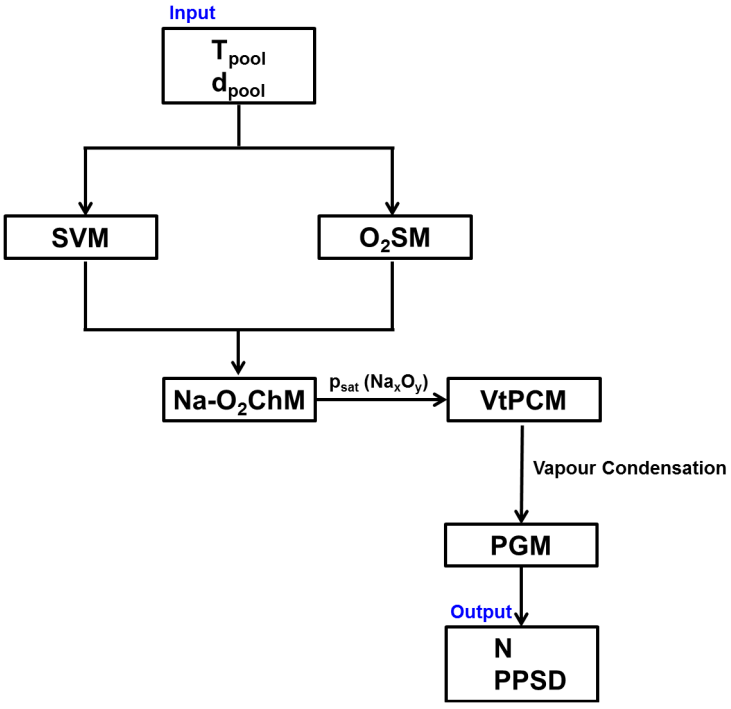

Fig. 2. PG model diagram.

generated particles (N) and the Primary Particle Size Distribution (PPSD) during an in-containment sodium pool fire.

3.1. Sodium vaporization model

In order to couple the liquid-sodium pool to the gas phase equations in FLUENT, the sodium vapour flux emerging from the sodium pool surface is needed as an input for the FLUENT simulation (Garcia et al., 2014).

Two approaches for the treatment of sodium pool combustion problem have been found in the literature. The first one, named as surface combustion model (Beiriger et al., 1973), is one in which Na vaporization rate is slow and Na-O_2 reactions occur at the pool surface. The second one, a gas-phase reaction model, was developed by Sagae and Suzuoki (1985) and later used by Miyake et al. (1991), Lee and Choi (1997), Doda et al. (2003), Yamaguchi and Tajima (2009), Karthikeyan et al. (2009) and more recently by Sathiah and Roelofs (2014).

According to the Na temperatures around 800 K in normal operating conditions in the primary and secondary circuit (IAEA, 2006), a sodium vaporization model to simulate gas-phase combustion is proposed.

Sodium vapour pressure is low at pool temperatures of 800–1000 K; therefore, a diffusion flame is established very close to the sodium surface. In this boundary layer, the diffusion of heat and mass is dominant and the convection can be neglected. Based on a diffusion layer approach, an expression for the molar flux of sodium vapour is derived. In the boundary layer (between pool surface and flame), one-dimensional sodium vapour diffusion is assumed taking into account the diffusive resistance of N_2 to the sodium vapour movement toward the flame. As boundary conditions, sodium vapour pressure is assumed to be saturated at the pool surface and to fall down to zero concentration at the flame region edge facing the pool; the latter means that Na disappears instantaneously as soon as it interacts with oxygen (infinite chemical-reaction rate). It is also assumed that oxygen penetration into the evaporating-sodium boundary layer is negligible due to its consumption in the flame; this allows the sodium-vapour flux boundary layer to be treated as a sodium-nitrogen binary-diffusion problem:

$$\phi_{Na} = -\frac{D_{Na}}{l_f}\cdot X_{Na}\cdot C_{bl}\cdot \ln\left(\frac{X_{N2,p}}{X_{N2,f}}\right) = \frac{D_{Na}}{l_f}\cdot X_{Na}\cdot C_{bl}\cdot \ln\left(\frac{P}{P-p_{sat,Na}}\right) \quad (1)$$

where the logarithmic term describes the diffusive resistance that N_2 presents to Na vapour diffusion. In this equation, correlations for the physical properties of Na from Fink and Leibowitz (1995) are used. Besides, a correlation for the diffusion coefficient of Na through N_2 from the SPRAY code (Shire, 1977) is used:

$$D_{Na} = 0.9998\cdot 10^{-9}\frac{T^{1.668}}{P} \quad (2)$$

The vaporized sodium molar flux equation (Eq. (1)) involves two unknown variables, the distance between the flame and the pool surface (l_f) and the flame temperature (T_f). To determine these, the mass and energy conservation equations at the flame are solved. In this approach, a number of hypotheses are considered: flame surface area facing the pool is equal to the pool surface area (i.e., flame surface is assumed to be smooth and parallel to the surface); all the gases are considered ideal; and pool temperature is supposed to remain constant as a function of time, i.e., the heat transfer of the foreseen oxide layer formed on the pool surface to the un-burnt sodium is neglected.

Mass balance at the flame is given by the following equation:

$$\phi_{Na} = X\cdot\phi_{O2} \quad (3)$$

where X is the oxygen-sodium stoichiometric ratio which is dictated by the chemical reactions described in Section 3.3 (Karthikeyan et al., 2009). In this equation, infinite rate chemistry is supposed, i.e., all the O_2 coming to the flame is instantaneously consumed by the Na vapour.

The supply of oxygen from the environment to the flame is driven by natural convection. As the Lewis number (Le = Sc/Pr, and defined as the ratio of thermal diffusivity to mass diffusivity) for this mass transfer system of sodium vapour and air becomes almost unity, the molar oxygen flux is determined by using the heat/mass transfer analogy (Nu/Sh):

$$\phi_{O2} = \frac{D_{O2}}{L}\cdot X_{O2}\cdot C_g\cdot Sh \quad (4)$$

where the McAdams correlations are used according to the scenario of interest (laminar/turbulent) (Bergman et al., 2011):

$$Nu = 0.54\cdot Ra^{1/4}\left(10^4 \leqslant Ra \leqslant 10^7, \mathrm{Pr} \geqslant 0.7\right) \quad (5)$$

$$Nu = 0.15\cdot Ra^{1/3}\left(10^7 \leqslant Ra \leqslant 10^{11},\ all\ \mathrm{Pr}\right) \quad (6)$$

Footnote:

The analytical calculation of the sodium flux is provided as an input for the numerical calculation. Once calculated, the oxygen transfer given by the O_2SM will be used to react with the vaporized Na in the numerical model.

The general heat equation at the flame can be expressed as follows:

$$m\cdot c_p\cdot\frac{dT_f}{dt} = E_{chem} + H_{gf} - E_{fNa}^{cond} - E_{fg}^{conv} - E_f^{rad} \quad (7)$$

where T_f is the flame temperature, E_{chem} is the combustion energy generated at the flame, H_{gf} is the enthalpy transferred by material fluxes of different species (sodium, oxygen and sodium oxides) to the flame, E_{fNa}^{cond} is the conductive-convective energy transfer from the flame to the pool surface, dominated by conduction, E_{fg}^{conv} is the conductive-convective energy transfer from the flame to the environment, and E_f^{rad} is the energy transfer by radiation from the flame to the pool surface and from the flame to the atmosphere and walls surrounding the pool.

The energy transferred from the flame by radiation influences combustion rate. According to Yamaguchi and Tajima (2006) studies on flame emissivities in sodium pool fires, the emissivity is strongly dependent on the aerosol cloud around the flame and it will increase at the start of the fire. The global heat transfer from the flame to the pool surface (conduction plus radiation) decreases over time because of the flame temperature drops due to the extra heat loss by radiation (Sagae and Suzuoki, 1985); therefore, the evaporation from the sodium pool surface decreases. Flame emissivity values have not been found in the open literature. Through numerical experiments, Yamaguchi and Tajima (2006) estimated flame emissivity from 0.2 to 0.8 depending on the boundary conditions (pool and gas temperatures and O_2 concentrations). Therefore, due to the high uncertainties in the flame emissivity, an estimation of the radiation effect on the sodium vaporized flux has been developed assuming maximum flame emissivity of 0.8. Furthermore, the maximum radiative transfer is fostered by considering view factors of unity. With these conditions of maximum radiation, variations in the sodium flux less than 10% have been found. Therefore, in steady-state conditions ($dT_f/dt = 0$) and by assuming no radiation from the flame, the energy balance at the flame can be approximated as:

$$E_{chem} + H_{gf} = E_{fNa}^{cond} + E_{fg}^{conv} \quad (8)$$

3.2. Oxygen supply model

The oxygen supply to the flame region is the consequence of natural convection over the flame region: given the significance that O_2 supply might have in the entire scenario and due to the extreme foreseen conditions above the combustion zone where high turbulence can be anticipated, a computational fluid dynamic model has been developed with the FLUENT 14.5 code (ANSYS, 2008). Several methodologies are available for the resolution of the Navier-Stokes equations in FLUENT. Direct solution of them (DNS) is not possible for the present problem due to the fine time and space resolution needed. Large-Eddy Simulations (LES) resolve only the large-scale turbulence and account for the smaller scales with subgrid-scale modelling. However, such simulations are still very onerous (of the order of weeks on an ordinary computer for rather simple flows). Finally, the Reynolds Averaged Navier-Stokes (RANS) methods fulfil the compromise between accuracy and computational costs (Andersson et al., 2012). With this model for steady-states, the equations of continuity, momentum and energy in Cartesian form can be written as follows:

Continuity:

$$\frac{\partial}{\partial x_j}\rho u_j = 0 \quad (9)$$

Momentum:

$$\frac{\partial}{\partial x_j}\rho u_i u_j = -\frac{\partial}{\partial x_j}P + \frac{\partial}{\partial x_j}(\tau_{ij} - \overline{\rho \mu_i' \mu_j'}) \quad (10)$$

Energy:

$$\frac{\partial}{\partial x_j}\left[\rho u_j\left(h_s + \frac{u_i u_j}{2}\right) + u_j P + q_j - u_i \tau_{ij}\right] = 0 \quad (11)$$

Turbulence effects have been simulated by adopting the SST k-ω model, as recommended by Menter (1994). In this model, the advantages of both k-ε and k-ω models are included (i.e., the robustness in the near wall-region of the k-ω model plus the accuracy of k-ε in the far field), which makes calculations computationally efficient in all regards.

The transport equations of the turbulent kinetic energy (k) and the specific dissipation rate (ω), together with the Boussinesq hypothesis to relate the Reynolds stresses to the mean velocity gradients close the system equations of continuity, momentum and energy are given by:

$$\frac{\partial}{\partial x_i}(\rho \cdot \phi \cdot u_i) = \frac{\partial}{\partial x_j}\left(\Gamma_\phi \cdot \frac{\partial \phi}{\partial x_j}\right) + G_\phi - Y_\phi(+D_\omega) \quad (12)$$

$$-\rho \cdot \overline{\mu_i' \mu_j'} = \mu_\tau\left(\frac{\partial u_i}{\partial x_j} + \frac{\partial u_j}{\partial x_i}\right) - \frac{2}{3}\left(\rho \cdot k + \mu_\tau \frac{\partial u_i}{\partial x_i}\right) \cdot \delta_{ij} \quad (13)$$

where ϕ denotes the independent variable (k and/or ω) and G, Y and Γ represent generation, dissipation and effective diffusivity of the given quantity, respectively. The set of equations are solved using a segregated implicit solver with a second-order discretization scheme.

3.3. Sodium-oxygen chemical model

A number of sodium pool fires experiments are reported in the literature. Hilliard et al. (1979) and Cherdron et al. (1985) performed large scale aerosol behaviour test in CSTF and FAUNA facilities, respectively. Malet et al. (1981, 1990) conducted sodium pool experiments to study the influence of sodium temperature, combustion area and atmosphere composition on the fire evolution. In all of them, the major species identified were oxide, Na_2O, and peroxide, Na_2O_2.

A more detailed analysis of the chemistry of sodium pool combustion was developed by Newman (1983) in his review of sodium pool fire tests carried out during the 1960s and 1970s. However, intermediate reactions and products were not clearly identified.

Based on the information found in the open literature on sodium pool fire analytical models (Sagae and Suzuoki, 1985; Marimuthu, 1996; Miyake et al., 1991; Lee and Choi, 1997; Karthikeyan et al., 2009; Yamaguchi and Tajima, 2009), two reactions are considered in the Na-O_2 chemical modelling:

$$Na + \frac{1}{4}O_2 \rightarrow \frac{1}{2}Na_2O + 316\ \text{kJ/mol} \quad (14)$$

$$Na + \frac{1}{2}O_2 \rightarrow \frac{1}{2}Na_2O_2 + 365\ \text{kJ/mol} \quad (15)$$

We note that some authors assert that reaction (14) is always the first oxidation step and, if there is sufficient oxygen, the sodium oxide produced is further oxidized to peroxide. In the present modelling and taking into account the very short time scale of interest for primary particle generation, formation of both oxide (Na_2O) and peroxide (Na_2O_2) are assumed to be infinitely fast, so that the relative proportion of each species in the products is governed by stoichiometry. That is, each 4 Na moles yield one mole of Na_2O and 1 mol of Na_2O_2; this means that in terms of mass fractions, of the total Na oxide species formed (Na_xO_y), around 40% is Na_2O and the remaining 60% is Na_2O_2.

During sodium pool combustion, the reaction of Na with the water vapour present in the atmosphere is also possible. However, as in most practical cases the oxygen is the major gas constituent, it is the oxidation by O_2 the dominating reaction (Yamaguchi and Tajima, 2003b, 2006). As a consequence, this reaction is not here considered.

For reacting flows, FLUENT provides several models for chemical species transport and chemical reactions. Among them, Generalized Finite-Rate Model is based on the solution of transport equations for species mass fractions, with the chemical reaction mechanism defined by the user. In this model, the conservation equations for chemical species are solved by predicting the local mass fraction of each species, Y_i, through the solution of a convection-diffusion equation for each species:

$$\frac{\partial}{\partial t}(\rho Y_i) + \nabla \cdot (\rho \vec{v} Y_i) = -\nabla \cdot J_i \rightarrow + R_i + S_i \quad (16)$$

The mass diffusion in turbulent flows is calculated in this model by the following expression:

$$J_i \rightarrow = -\left(\rho D_{i,m} + \frac{\mu_\tau}{Sc_t}\right)\nabla Y_i \quad (17)$$

The reaction rates that appear as source terms in the convection-diffusion equation (R_i) are computed by the eddy-dissipation model in which the reaction rates are assumed to be controlled by turbulence mixing and the Arrhenius chemical kinetic is not calculated. This model can be selected assuming Na-O_2 reactions are infinitely fast (Miyake et al., 1991). The net rate of production of species i due to reaction r, $R_{i,r}$, is given by the smaller of the two expressions below:

$$R_{i,r} = \nu_{i,r}' M_{w,i} A \rho \frac{\varepsilon_T}{k} \min_R\left(\frac{Y_R}{\nu_{R,r}' M_{w,R}}\right) \quad (18)$$

$$R_{i,r} = \nu_{i,r}' M_{w,i} A B \rho \frac{\varepsilon_T}{k} \frac{\sum_P Y_P}{\sum_j^N \nu_{j,r}'' M_{w,j}} \quad (19)$$

The default values in the code for the empirical constants A and B have been used (A = 4.0 and B = 0.5).

3.4. Vapour-to-particle conversion model

As stated by Newman (1983), the combustion mechanism between sodium vapour and oxygen in the gas phase is followed by the formation of a condensed oxide by homogeneous and heterogeneous nucleation.

Once the supersaturated vapours have been formed in the gas phase after sodium oxidation, the system is in a non-equilibrium state. To reach equilibrium, the surplus of vapour molecules condenses (homogeneous nucleation) forming primary clusters on which other vapour molecules might condense (heterogeneous nucleation).

3.4.1. Homogeneous nucleation

Homogeneous vapour-liquid nucleation is a fundamental mechanism of phase transformation. The nucleation process involves formation of clusters in a metastable bulk vapour by thermal fluctuations: the transition from a metastable state over an energy barrier for the system to reach its thermodynamic equilibrium.

Even though nucleation has been studied since the 18th century, a reliable theoretical formulation has been difficult to derive. Major reviews of nucleation modelling exist (e.g. Kashchiev (2000), Ford (2004), Vehkamäki (2006)). Based on these, a diagram of evolution of nucleation theories is shown in Fig. 3. According to the scheme, Transition State Theory (TST) can be considered as the first theory of nucleation (Ford, 2004). Within the framework of the free-energy fluctuations theory, the probability of forming a critical cluster is exponentially related to the Gibbs free energy of cluster formation. The proportionality constant in the nucleation rate equation was included by Volmer and Weber (1926) by their kinetic interpretation of nucleation phenomena: nucleation is understood as a set of collisions, and the only important transitions are those that are brought about by the addition or loss of single molecules to form the cluster. The theory of Volmer and Weber was extended a few years later by Becker and Döring (1935), Farkas (1927) and Zeldovich (1942) is now known as Classical Nucleation Theory (CNT). From the CNT, the evolution of analytical nucleation theories has been driven through two main branches (Fig. 3). On one side, adjustments of the CNT with "minor" corrections (phenomenological approaches); on the other, approaches developed for a more exhaustive description from the microscopic point of view. Among the microscopic theories, there are two main streamlines. On one side, the approaches based on defining a cluster by imposing geometric constrains on the molecular positions (Stillinger, 1963; Senger et al., 1999); on other side, the Density Functional Theory (DFT) (Oxtoby and Evans, 1988; Oxtoby, 1998) in which the key assumption in the phenomenological approaches – capillarity approximation – is removed and the free-energy barrier to nucleation is calculated in a non-classical manner using a mean field theory in which the molecules forming the cluster move in an effective potential field created by the other molecules in the cluster (Ford, 2004).

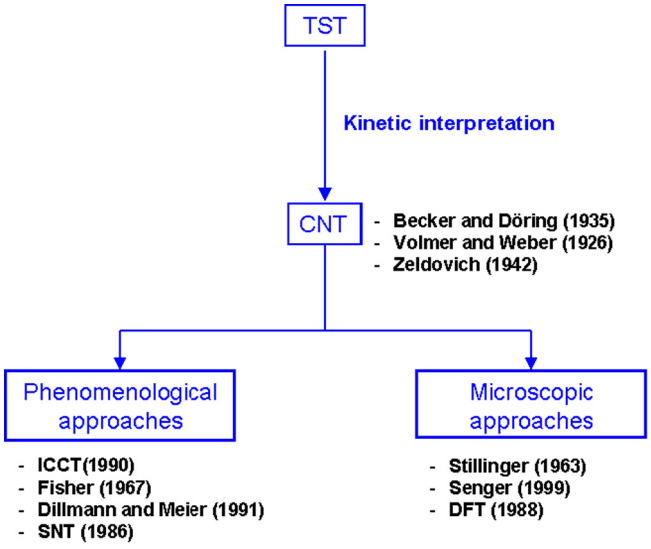

Fig. 3. Overview of the main analytical theories on homogeneous nucleation.

The simplest phenomenological adjustment is the Internally Consistent Classical Theory (ICCT) developed by Girshick and Chiu (1990) in which an unevaluated normalization constant in the nucleation rate expression is introduced. The Fisher droplet model (1967) is a slightly more sophisticated approach in which parameters are introduced in the free-energy barrier to nucleation to ensure that the model correctly reproduces known properties of clusters and vapours, including virial coefficients and critical properties. Dillmann and Meier (1989) developed a model based on the Fisher model using the observed critical-vapour properties and the second virial coefficient. The model is based on considering the curvature dependence of the droplets surface tension and additional degrees of freedom in the definition of the Gibbs free energy variation. However, the success of this model is challenged by correction of an inconsistency that leads to large changes in the predicted nucleation rate, Ford et al. (1992). Finally, Scaled Nucleation Theory (SNT), proposed by Hale (1986), is based on CNT but employing simplified models for the surface tension and liquid density based on scaled behaviour near the critical point.

Based on the review and analysis of the available models in the literature, it has been concluded that Classical Nucleation Theory (CNT) might be a suitable approach for the assessment of the nucleation rates in the case of an in-containment sodium-pool fire. The higher complexity of other theories, the inherent uncertainty coming from the lack of information on Na_xO_y properties and the huge sensitivity of any homogeneous nucleation theory to variations in boundary conditions (i.e., temperature) are the main supporting reasons for this choice. In addition, the complexity of other theories entails an extra numerical burden and the supposed gain in accuracy vanishes due to the intrinsic uncertainties in additional properties and estimation of key variable.

The CNT considers that the probability of attaining a cluster of a critical size (minimum number of particles to form a stable cluster) is exponentially related to the energy necessary to form it. The expression of the nucleation rate derived from the work of Becker-Döring, Frenkel, Farkas and Zeldovich is given as:

$$J_{CNT} = J_0 \cdot \exp\left[-\frac{\Delta G^*}{k_B T}\right] \tag{20}$$

where the energy barrier to form a cluster (ΔG^*) is the minimum of the classical Gibbs free energy for the formation of a droplet. The change of Gibbs free energy (ΔG) is the difference between a mechanical term proportional to the surface tension (associated with the creation of a spherical interface) and a thermal term proportional to the logarithm of the saturation ratio of the free vapour (coming from the difference in the Gibbs free energy of the liquid and vapour states, i.e., the phase change from supersaturated vapour to condensate) (Seinfeld and Pandis, 2006):

$$\Delta G = 4\pi \cdot r^2 \cdot \sigma - ik_B T \ln S \tag{21}$$

where i is the number of molecules forming the cluster and S is the saturation ratio ($S = p_{vap}/p_{sat}(T)$). This expression relies on the

capillarity approximation that considers extremely small particles with the same surface tension as a liquid planar surface.

Therefore, the nucleation rate expression in CNT is as follows:

$$J_{CNT} = \left(\frac{2\sigma}{\pi m_1}\right)^{1/2} \cdot v_1 \cdot N_1^2 \cdot \exp\left[-\frac{16\pi}{3} \cdot \frac{v_1^2\sigma^3}{(k_B T)^3 (\ln S)^2}\right] \quad (22)$$

This expression can be explained as formed by two contributions. On one side, the pre-exponential factor involves specific features of the kinetics of the process as the collision probability of individual vapour molecules with critical clusters of the new phase. On the other side, the exponential factor reflects the thermodynamic aspects of the theory: the thermodynamically stable phase corresponds to the minimum Gibbs free energy of formation that represents the barrier for the transition of the system into the new phase.

The critical particle size is obtained by applying the extreme condition in the Gibbs free energy of formation ($[d\Delta G/dr]_{r^*} = 0$):

$$r^* = \frac{2\sigma v_1}{k_B T \ln S} \quad (23)$$

3.4.2. Condensation

The growth mechanism of condensation on existing particles has been extensively documented in the literature (e.g. NEA (2009), Friedlander (2000), Seinfeld and Pandis (2006), Hinds (1999)). The rate of aerosol growth by condensation will depend on the saturation ratio, particle size and particle size relative to the gas mean free path (Hinds, 1999). For particles much larger than the mean free path (Knudsen number lower than unity, Kn < 1.0), the rate of condensation is controlled by the rate at which vapour can diffuse toward the particle surface. However, for particles much smaller than the mean free path (Kn ≫ 1.0), the rate of particle growth by condensation will be governed by the rate of random molecular collisions between the particle and the vapour molecules. It is noted that Fuchs and Sutugin (1970) developed a formulation covering both the high and low-Knudsen number ranges including the transition regime.

As the critical particles generated by homogeneous nucleation are foreseen to be in the order of nanometres (NEA-CSNI, 1979), the prevailing conditions for heterogeneous nucleation fall in the free molecular regime (i.e., $Kn = 2\lambda/d_p \gg 1.0$). Therefore, the removal of vapours by condensation is calculated as the net flow of molecules attached to the surface of a particle of a given size by collisional impact (kinetic theory). In this formulation, the condensation rate can be expressed as:

$$F = \frac{z \cdot a}{N_{AV}} \approx \frac{\pi d_p^2}{(2\pi m_1 k_B T)^{1/2}} (p_{vap} - p_{sat}) \quad (24)$$

In this expression, the Kelvin effect, i.e., the effect of surface curvature is neglected as a simplification (Friedlander, 2000). During condensation, particle latent heat is released at the particle surface. In these conditions, convection is an inefficient means of heat transfer since the particles are very small and move with little slip along with the gas; the same occurs with radiation since all the particles have roughly the same temperature. Otherwise, conduction through the gas phase is available for heat removal from the particle surface where condensation is taking place, so condensation might be limited by the rate of heat removal from the particle surface. In our approach, however, the reduction of the condensation-rate due to the rise in the temperature from the release of latent heat has not been taken into account as no data on Na_xO_y diffusion coefficients are found in the available literature. These approximations (neglect of both curvature and latent heat) might lead to an over-estimation of the arrival of vapour molecules to the droplet surface, i.e., an over-estimation of the condensation.

By considering the rate of change of particle volume as:

$$\frac{dV}{dt} = F \cdot v_1 \quad (25)$$

The resulting particle size is given by the following growth law expression (Friedlander, 2000):

$$\frac{dd_p}{dt} = \frac{2v_1}{(2\pi m_1 k_B T)^{1/2}} (p_{vap} - p_{sat}) \quad (26)$$

In this approach, growing particles are assumed to remain in kinetic-regime conditions. During the initial stages of particle growth, this can be considered as an adequate approximation since condensation occurs on sub-micrometre particles coming from homogeneous nucleation (Shaw, 1989).

3.4.3. Vapour-to-particle conversion

As shown in previous sections, vapour pressure is a key variable defining any particle formation in a supersaturated vapour. Homogeneous nucleation will reduce the number of free condensing molecules available and, hence, vapour pressure. But also, heterogeneous nucleation drivers will bring vapour molecules onto primary particle surfaces where they condense and further reduce vapour pressure.

Therefore, the total number of particles formed will be given by the nucleation and condensation as simultaneous and competitive processes (Warren and Seinfeld, 1984; Clement and Ford, 1999a,b). Given that both processes are very fast, their full modelling (i.e., both phenomena competing for vapour molecules as a function of time) is an onerous computational burden since, for each time step, both nucleation and condensation should be calculated on a particle size distribution that would become more dispersed as time progresses. Instead, one may assume that after the first homogeneous nucleation, heterogeneous nucleation dominates from that time onward. In other words, this second approach neglects homogeneous nucleation beyond the first burst of primary particles. Both approximations are outlined in Fig. 4.

Fig. 5 shows the number of generated particles by both approaches for a sodium pool fire of radius 5 cm (pool temperature of 1000 K and 21% of initial O_2 content). From the figure, the realistic approach (nucleation-condensation model) results are 3 times larger than the single-burst approach. In the first one, it can be observed that from the first nucleation at 10^{-8}s, there is an abrupt increase in the generation of particles until $1.1 \cdot 10^{-7}$ s, reaching a value of $1.71 \cdot 10^{20}$ particles. At this point, there is no further particle formation due to the depletion of Na_xO_y vapour down to its saturation pressure by homogeneous nucleation and condensation, i.e., the nucleation process is cut-off. In the second one, however, homogeneous nucleation gives $5.13 \cdot 10^{19}$ particles at the start of the calculation. Both approaches agree with the idea of Clement and Ford (1999a,b): particle production takes place in occasional and isolated bursts of nucleation and as foreseen, all the generated oxides produced during the sodium oxidation seem to be in particle form after a short period of time, of the order of 10^{-7} s. Concerning primary-particle size, as conditions in each cell of the domain are different, a few cells of the domain covering the entire conditions range were picked and both approximations compared; the approximate result was that both predictions give diameters in the nano-range, but with the diameters in the realistic approach approximately twice as larger as those in the single-burst approach.

As these estimates are strongly affected by uncertainties, a simple estimation of the error propagation linked to the properties used in the nucleation formulation has been developed to evaluate

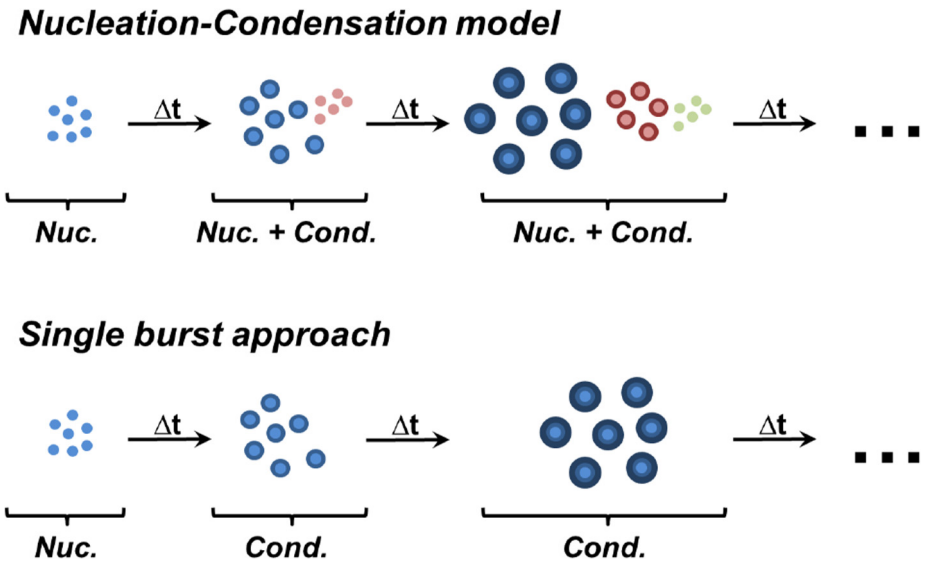

Fig. 4. Nucleation approaches.

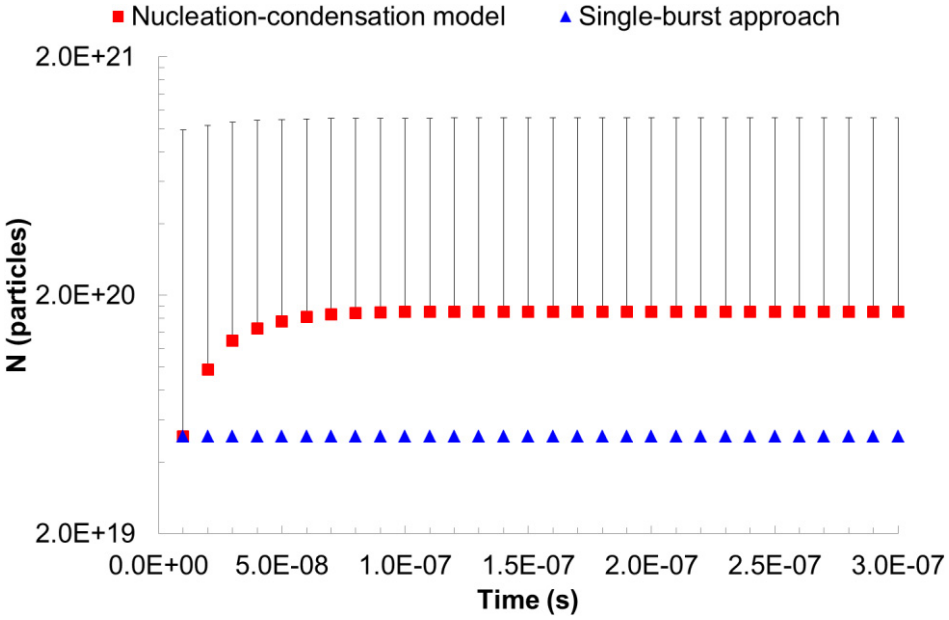

Fig. 5. Total number of generated particles by the two modelling approaches.

the minimum bands of uncertainties in the number of generated particles. Uncertainties associated to the theoretical expressions of homogeneous nucleation are not considered. Following the error propagation theory, the nucleation-rate expression uncertainties are calculated by the following expression:

$$\sigma^2_{J_{CNT}} = \left(\frac{\delta J_{CNT}}{\delta \sigma}\right)\sigma^2_{\sigma} + \left(\frac{\delta J_{CNT}}{\delta p_{sat}}\right)\sigma^2_{p_{sat}} + \left(\frac{\delta J_{CNT}}{\delta \rho}\right)\sigma^2_{\rho} \quad (27)$$

where the density and surface tension errors are evaluated based on the available information in the open literature (Janz, 1988). Regarding saturated-vapour pressure, the error has been evaluated based on the maximum difference found between the two available correlations (Jacq, 2006; Lamoreaux and Hildenbrand, 1984).

An upper uncertainty bound up to 2 orders of magnitude has been estimated. Therefore, by considering the estimated large uncertainties associated with the homogeneous nucleation model, we consider the single-burst approach to be accurate enough to describe the vapour-to-particle conversion process.

In this approach, the Na_2O and Na_2O_2 correlations of saturated-vapour pressure, density and surface tension as a function of temperature are needed to calculate the number of generated particles by homogeneous nucleation and its growth. As no information on Na_2O_2 density and surface tension is found, in this model both oxides are characterized by the same properties, i.e., both Na_2O and Na_2O_2 are treated as indistinguishable Na_xO_y as far as nucleation and condensation are concerned. Then, the correlations we use are the Na_2O saturated-vapour pressure proposed in Jacq (2006); regarding density and surface tension and in the absence of specific correlations for Na_2O, correlations for Na_2CO_3 are used (Janz, 1988).

4. Results

The available data in the literature to conduct a full and extensive validation of the model presented in previous sections, in terms of particle number and size, are scarce. Nonetheless, some measurements concerning the burning rate have been found and the model will be compared with these (next section). Then, the model performance will be assessed in a scenario whose conditions reflect those expected in the case of a realistic Na pool fire.

4.1. Partial validation

A partial validation of the PG model has been carried out based on the sodium pool experiments of Newman and Payne (1978). For benchmarking, estimates of burning rates based on the surface model included in SOFIRE code (Beiriger et al., 1973) have been added. SOFIRE is a reputable sodium pool combustion model based on the surface combustion approach (i.e., no Na vaporization is accounted for).

In Newman and Payne's experiments, the burning rates of sodium pool fires were measured for a sodium pool of 0.1 m diameter at sodium pool temperatures in the range of 523–1023 K and in natural-convection airflow conditions (oxygen molar fraction of 21%). Burning rates were measured by measuring the sodium pool mass change with time and by collecting the emitted smoke using a pumped filtering system.

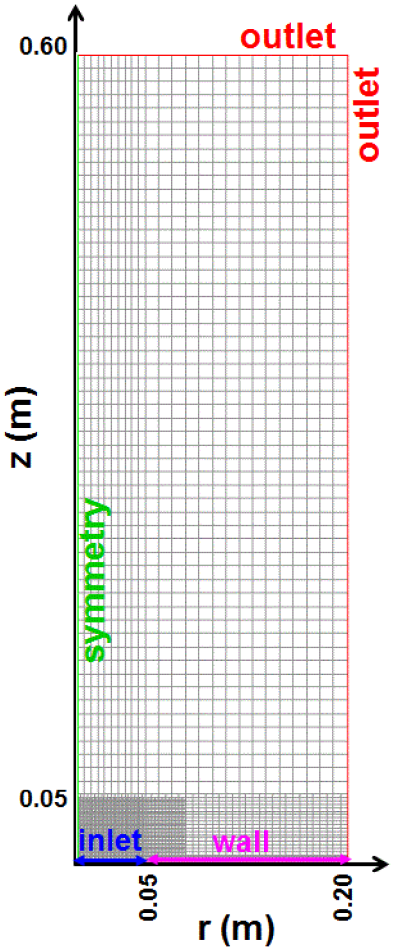

Fig. 6. Meshing of the sodium fire simulation.

The circumferential symmetry of the experimental scenario allows assuming circumferential symmetry (i.e., the same variables profiles are expected at any azimuth). The geometry and domain meshing of the problem is illustrated in Fig. 6. The sodium pool is represented by a surface of 0.05 m radius. It is worth reminding that in this approach, the liquid sodium pool is modelled as a steady thermal surface; i.e., the sodium pool is assumed to be fully stagnant (i.e., no spreading considered). The computational domain is rectangular, with 0.60 m height and 0.20 m length. The ratio of the pool surface area to the horizontal cross-sectional area of the domain is 0.065 which ensures that pool combustion is not influenced by the size of the domain; in other words, the vessel size does not influence the O_2 supply by natural convection over the horizontal combustion plane (Sagae and Suzuoki, 1985). For the non-uniform grid, 4001 quadrilateral cells are used to mesh the entire volume. The largest areas of nodes are outside the flame zone (c.a., 10^{-2} m^2); contrarily, within the flame region the mesh grew and much smaller cells were considered (10^{-6} m^2).

Fig. 7 compares the calculated burning rates of liquid sodium with the experimental results of Newman and Payne (1978). In addition, the Na burning rates calculated by the surface combustion model SOFIRE are included. Note that pool temperatures in the figure are over 800 K (i.e., in the gas-phase combustion regime).

From Fig. 7, the estimates-to-data agreement is outstanding. On the one hand, the experimental trend of increased burning rate with Na pool temperature is followed by the calculations. On the other hand, the data scattering helps predictions to be well within the measurements range. As can be observed, SOFIRE noticeably under-predicts the burning rates. Probably the major difference between both approaches concerns reaction temperatures: whereas in the gas-phase-combustion approach (PG model) the flame temperature is always higher than the pool one (1300 K and 1000 K according to Newman and Payne, 1978), the surface combustion approach takes the pool temperature as the reaction temperature. This temperature discrepancy makes a difference in terms of reaction rates (Sagae and Suzuoki, 1985). In addition, oxygen transfer by natural convection to the flame will be fostered by the higher temperatures at the flame what, in turn, will lead to faster combustion.

These results seem to indicate that surface combustion is not conservative when applied at pool temperatures over 800 K since it would under-predict both the thermal load to the containment and the airborne-particle loading relative to what could be expected in the case of an in-containment pool fire.

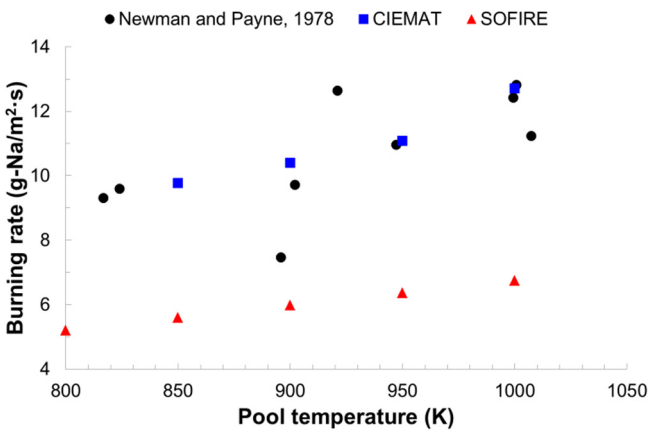

Fig. 7. Burning rates vs. pool temperature.

4.2. PG model estimates

4.2.1. Main results

In order to show the PG model performance, a scenario thermally similar to the one foreseen in the case of a pool fire (i.e., atmospheric pressure and pool temperature of 1000 K) has been proposed in a geometry similar to the one used in Newman experiments (i.e., a 10 cm Na-pool diameter).

The velocity field is shown in Fig. 8a. The general flow pattern is an ascending flow entering from the edge of the pool surface. The ascending flow velocity distribution behaves like a plume: low horizontal velocities at the reaction zone (edge of the pool surface) and upward velocity increasing towards pool centre (maximum velocity of 1.185 m/s at 0.06 m above the pool surface at the centre) due to buoyancy forces mainly driven by temperature gradients. Inside the plume, velocities of 0.70 m/s are reached. Note that O_2 concentration drops in the air stream as oxygen is partially depleted while the flow moves towards the pool centre (Fig. 8b).

More linked to the particle generation are temperatures and Na-oxides partial pressures. The temperature field is shown in Fig. 9a. Sodium burning starts at the edge of the pool surface due to fresh air entering into contact with sodium vapour by natural convection. The sodium-vapour combustion generates an ascending plume from the edge of the pool surface to the centre. A maximum temperature spot of 1448 K is produced where the oxidation starts while the temperature decreases along the plume to 1200–1300 K at 0.03 m from the pool centre. These estimates reasonably agree with the measurements made by Newman and Payne (1978) of 1300 K at the flame. In Fig. 9b, molar concentrations of Na_xO_y are shown. As can be observed, the region of higher concentrations is just above the sodium pool surface; nonetheless, it should be realized that location of the highest oxide concentration will depend on Na vaporization rates and O_2 supply rates, so that at high vaporization rates in O_2-poor atmospheres, the highest oxide region might not be so close to the pool surface. Also, the Na_xO_y upward diffusion can be distinguished.

Even though, particle generation rates heavily depend on temperatures and partial pressures, much of such a dependence is made through the saturation ratio, which essentially indicates how high Na_xO_y vapour pressures are with respect to those at thermal equilibrium (p_{sat}). Vapour pressures of Na_xO_y are calculated from the molar concentrations by assuming ideal gas behaviour. In order to focus on the region of interest (active volume), a criterion has been adopted: sodium-oxide vapour pressure must be higher than the saturated-vapour pressure of sodium oxides at the boiling temperature (1153 K).

Due to the extremely low values of the saturated-vapour pressure of the oxides, large values of S are found in the analysed region; it is worth highlighting the large gradients of S found, with values from 10^4 to $1.6{\cdot}10^{20}$ (Fig. 10). Maximum partial pressures are reached in the flame region; more specifically, just above the pool surface. On the other hand, saturated-vapour pressure is an increasing function of temperature. Therefore, the lower S values are reached just above the pool surface. In this region, in spite of the large concentrations of Na_xO_y, the large values of saturated-vapour pressures due to the large temperatures dominate the saturation ratio. In the region near the pool centre (x = 0.010), just above the pool, the saturation ratio slowly decreases up to 0.01 m height due to the decrease in the molar concentrations. Above this distance over the pool, a decreasing trend in the saturation ratio is observed due to both factors: on the one hand the decrease of molar concentration and then of partial pressure, and on the other hand the temperature increase at 0.02 m height above the pool centre.

Finally, Fig. 11 shows the particle concentration in the active volume obtained by integration over time of the nucleation rate in all the cells forming the active volume. As expected, the highest particle concentration is found in the flame region, and more specifically, just above the pool surface. This is due to the high Na_xO_y partial pressures right above the pool in relation to the high temperatures also reached in that area (saturation pressure is an increasing function with temperature). By summing the particle concentration for all the cells, huge concentrations of particles are produced during a sodium pool fire, of the order of 10^{26} particles for this scenario and the characteristic time to attain equilibrium would be of the order of 10^{-7} s. At such high concentrations, the usual consideration that particle concentrations are dilute allowing aerosol models to assume independent gas and particle phases breaks down; strictly, the classic approximation should be abandoned since things such as the effective density of the gas-particle phase and the turbulence itself are changed.

As noted in the graph, in less than 10 cm of height over the Na pool, the particle generation rate reduces to less than 10% of the maximum intensity. This means that in SFR containments particle generation from pool fires would be a sort of local phenomena

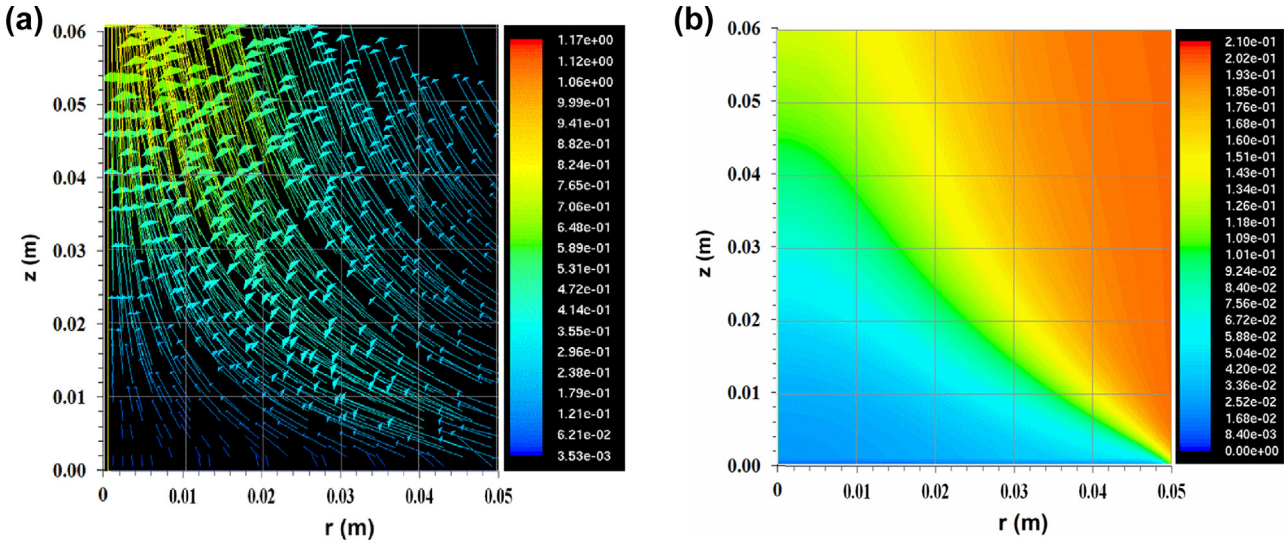

Fig. 8. (a) Flow velocities field (m/s). (b) O_2 mass fraction field.

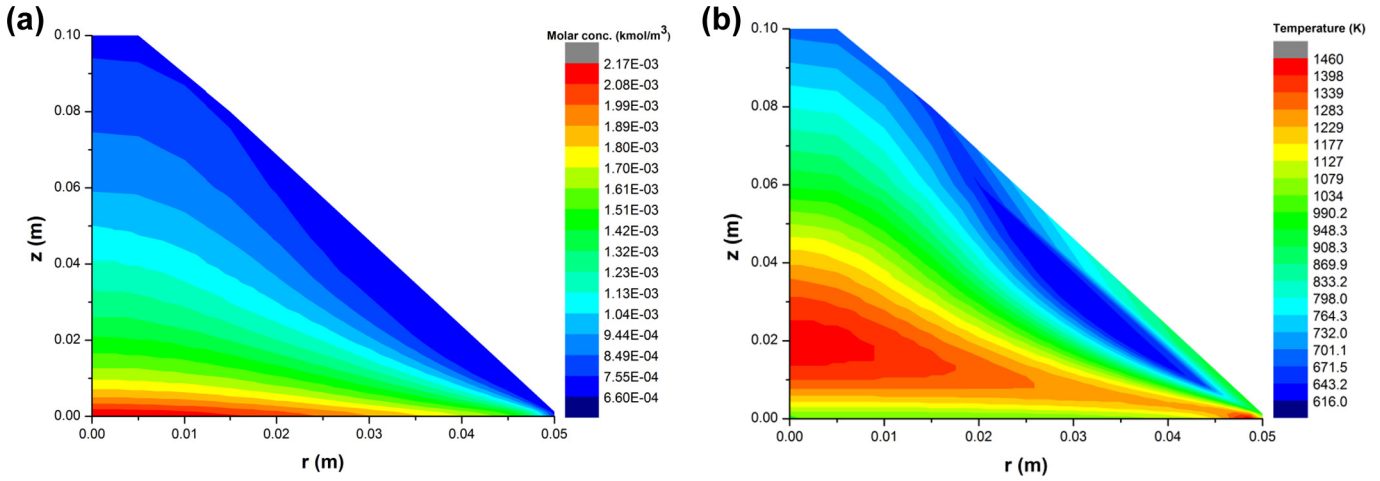

Fig. 9. (a) Temperature field (K). (b) Na_xO_y molar concentration (kmol/m^3).

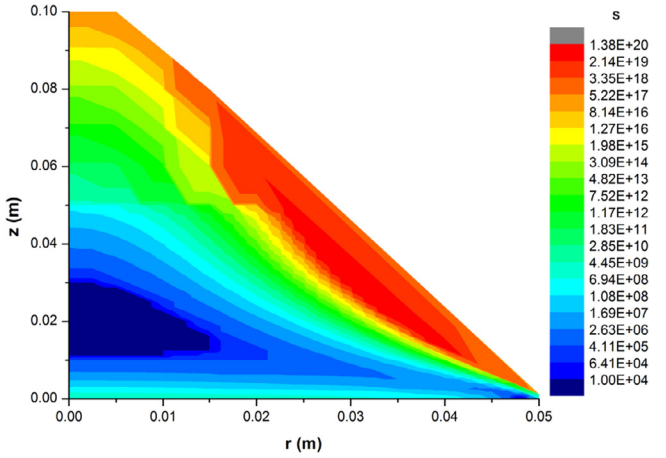

Fig. 10. Saturation ratio map at the analysed region.

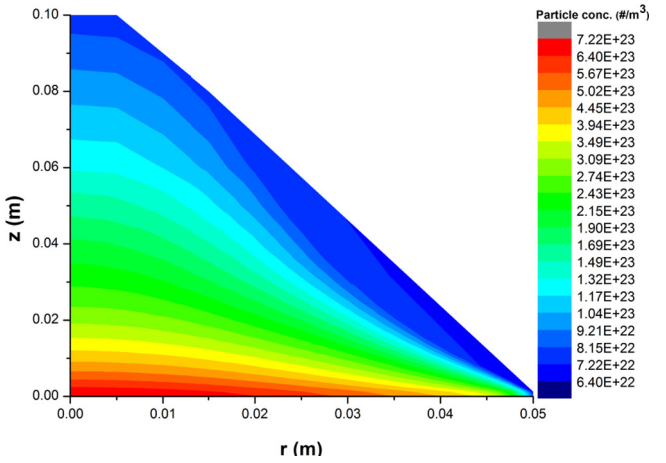

Fig. 11. Particle concentration map (particles/m^3).

practically restricted to a small region over the pool. Out of this region (the active volume), unrealistic values of S prevent the particle generation calculation. This observation is highly relevant for a future adaptation of the PG model to a SFR safety simulation code as ASTEC-Na (Girault et al., 2015) since, to a good approximation, particle generation can be confined to a relative small containment volume right above the Na pool surface.

The primary-particle size distribution is presented in Fig. 12. Primary particles present very small diameters hardly reaching the nano-range in a sharp distribution in which most particles fall between $6.5{\cdot}10^{-10}$ m and $8.7{\cdot}10^{-10}$ m for the scenario proposed here. These values are consistent with the embryos sizes reported in NEA-CSNI (1979). While increasing supersaturation reduces critical-particle size, and in our problem high supersaturations occur, this very small size implies clusters are stable when corresponding to just a few Na_2O molecules.

4.2.2. Parametric study of the PG model

A parametric study has been developed to analyse the influence of the main variables physically related to the governing phenomena in the anticipated scenario: pool diameter (from 0.1 m to 10 m), as the characteristic system dimension for natural convection and pool temperature (from 850 K to 1000 K), main driver for the Na evaporation from the pool. In all the cases, ambient normal conditions are considered. Table 1 synthesizes the discrete values selected to build up a total of 32 cases.show the calculated total number of particles N versus the analysed variable (pool temperature and pool diameter) for all the foreseen scenarios.

The dependencies of the calculated total number of particles (N) with sodium pool temperature and sodium pool radius (the macroscopic variables defining the scenario) for all the foreseen scenarios

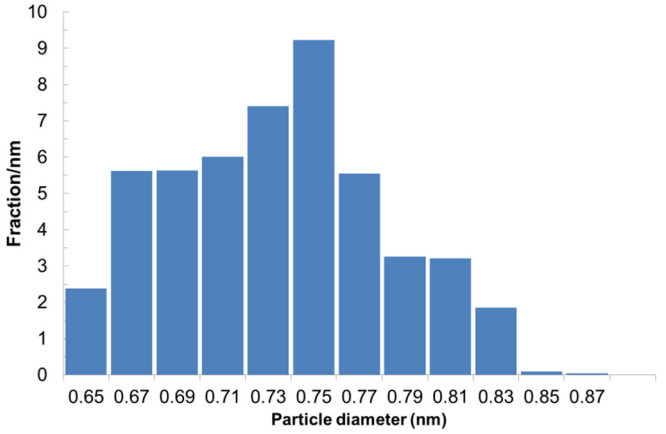

Fig. 12. Primary particle size distribution.

Table 1
Tests matrix.

Key variable	Range	Cases
Pool diameter	From 0.1 m to 10 m	0.1, 0.2, 0.5, 1.0, 2.0, 5.0, 7.5, 10.0
Pool temperature	From 850 K to 1000 K	850, 900, 950, 1000

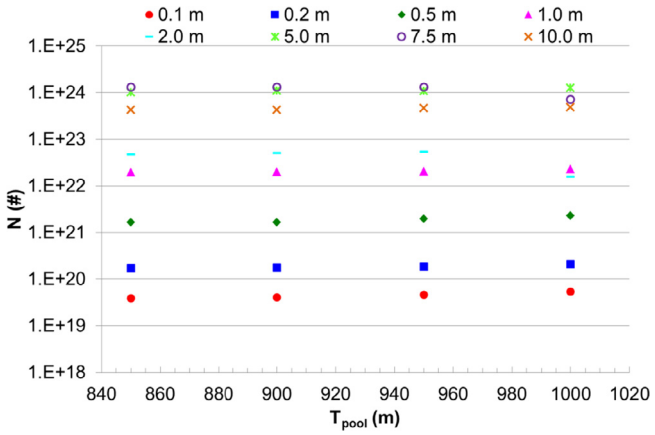

Fig. 13. Particle number vs. Na-pool temperature.

are analysed in Figs. 13 and 14. From the figures, it can be observed that the number of generated particles hardly depends on pool temperature (Fig. 13); however, a simple potential correlation with $R^2 > 0.99$ could be found for the dependence of N with sodium pool radius (Fig. 14).

4.3. Impact of agglomeration in the PG model

PG model predicts large concentrations of small particles in the close vicinity of a pool. Furthermore, a high level of turbulence is calculated in this area with turbulent-energy dissipation rates of the order of tens $J\,kg^{-1}\,s^{-1}$. In these conditions, turbulence-induced particle agglomeration could lead to a reduction in the total number of particles and to an increase in the average size (Friedlander, 2000). Therefore, it is necessary to evaluate the impact of agglomeration (turbulent and Brownian) on PG model estimates. Two possibilities are envisioned depending on the characteristic time of agglomeration compared to the particle-generation one: the first one is that particle generation takes place on a much faster timescale than agglomeration and the PG model does not need in this case to include agglomeration phenomena; the second one is that both particle generation and agglomeration occurs on similar timescales, then PG model would need to include the influence of agglomeration.

To evaluate the impact of agglomeration in the PG model, the characteristic time of both Brownian and turbulent agglomeration is calculated in the case of a sodium pool fire of radius 5 cm (pool temperature of 1000 K and 21% of initial O_2 content) by the equation:

$$t_c = \frac{2}{C \cdot \beta} \tag{28}$$

where C is the particle concentration predicted by the PG model and β is the collision frequency function or kernel (m^3/s).

In the free molecular regime, the Brownian agglomeration kernel can be calculated by (Friedlander, 2000):

$$\beta_{Brownian} = \left(\frac{3}{4\pi}\right)^{1/6} \cdot \left(\frac{6k_B T}{\rho_p}\right)^{1/2} \cdot \left(\frac{1}{v_i} + \frac{1}{v_j}\right)^{1/2} \cdot \left(v_i^{1/3} + v_j^{1/3}\right)^2 \tag{29}$$

where the subscripts i, j denotes particle classes.

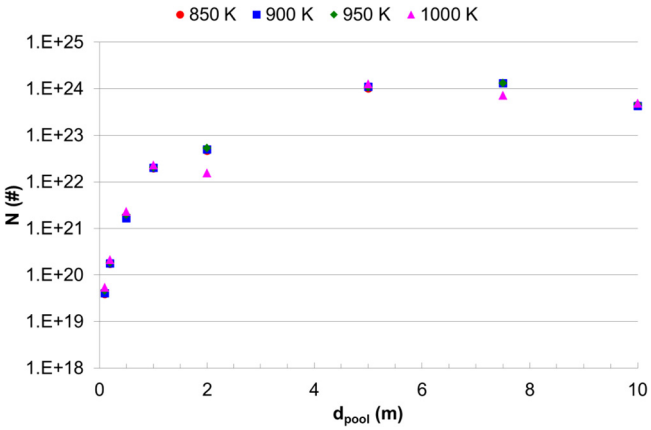

Fig. 14. Particle number vs. Na-pool diameter.

For the turbulent agglomeration, the collision-frequency function is calculated by considering the shear and inertial effects (MELCOR):

$$\beta_{Turbulent} = c_s \cdot \left(\beta_{Shear} + \beta_{Inertial}\right)^{1/2} \tag{30}$$

where the shear effect is due to the relative movement of particles by their different velocities in the eddies (Saffman and Turner, 1956; SNL, 2015):

$$\beta_{Shear} = \left(\frac{\pi \cdot \varepsilon_T \cdot \rho_g}{120 \cdot \mu}\right)^{1/2} \cdot \left(\gamma_i \cdot d_i + \gamma_j \cdot d_j\right)^3 \tag{31}$$

and the inertial effect is due to the relative motion of particles by their different mass (Saffman and Turner, 1956; SNL, 2015):

$$\beta_{Inertial} = \frac{0.04029 \cdot \rho_g^{1/4} \cdot \varepsilon_T^{3/4}}{\mu^{5/4}} \cdot \left(\gamma_i d_i + \gamma_j d_j\right)^2 \cdot \left|\frac{\rho_{pi} C_i d_i^2}{\chi_i} - \frac{\rho_{pj} C_j d_j^2}{\chi_j}\right| \tag{32}$$

As can be observed, these equations rely on the turbulent energy dissipation rate (ε_T) whose value has large uncertainties and greatly depends on the conditions evaluated. For example, the default value for the containment atmosphere during a severe accident of a water-cooled reactor in the MELCOR code (SNL, 2015) is 10^{-3} m^2/s^3. However, $\varepsilon_T \sim 10$ is predicted in the flame region just above the pool surface in the developed numerical simulation.

At the given conditions and by considering two particles colliding where one of these particles has a diameter two times larger than the other one, characteristic times of turbulent agglomeration (10^3 s) much longer than predicted times for particle generation (10^{-7} s) are obtained; hence, turbulent agglomeration should not affect PG model estimates. However, characteristic times for Brownian agglomeration only two times longer than particle generation times are calculated in these conditions. Hence, in the case of small pools, Brownian agglomeration could affect the PG model results.

5. Conclusions

Among the postulated Beyond Design Basis Accidents (BDBAs) in Sodium-cooled Fast Reactors (SFRs), the contaminated-coolant discharge at high temperature into the containment is considered as a potential dimensioning event during severe accident progression in terms of energetics and source term. In this scenario, the low saturation pressure of released sodium leads to its strong vaporization. As a consequence of the high chemical reactivity of sodium with oxygen, this would undergo oxidation and large

quantities of activated and contaminated particles would subsequently form by nucleation of the combustion products. Thus, nucleation of particles from supersaturated vapours is envisioned as the most important source of aerosols into the containment during a sodium fire in SFRs. From the safety point of view, it is of utmost importance to have computational tools properly validated, particularly in the field of radionuclide transport in the containment. In this context, several computer codes have been developed in the past to analyse these scenarios although they have mostly focused on energetics and thermal-hydraulics (Murata et al., 1993) so that particle modelling has received much less attention. For example: the SOFIRE code (Beiriger et al., 1973) assumes that all sodium-oxides produced becomes particles of a given size with no consideration of particle formation kinetics or primary-particle size. This paper presents the main features and bases of a Particle Generation (PG) model whose main output variables are the particle generation rate and the primary particle size during an in-containment sodium pool fire.

The particle formation process over a high temperature pool of Na (T > 800 K) requires the modelling of both thermal phenomena (i.e., Na vaporization from the pool surface and oxygen natural circulation from the atmosphere to the reaction zone) and physico-chemical phenomena (i.e., Na-oxygen chemical reactions and homogeneous and heterogeneous nucleation of sodium oxides vapours).

Based on a diffusion-layer approach, an expression for the flux of sodium vapour from the pool surface is given by taking into account the diffusive resistance of nitrogen to the sodium vapour movement toward the flame and assuming no sodium vapour concentration in the flame region. The binary diffusion model can be used because most of the oxygen is removed by chemical reactions and so is present at very low concentrations between the pool and the flame. Through this, a dominant link of sodium vapour flux from the pool surface with the sodium pool temperature can be established.

The saturation-ratio estimation over a sodium-pool combustion scenario determines when and where the nucleation process is possible during in-containment sodium-pool combustion. Due to the expected extreme boundary conditions over the pool at the time of oxidation, a partially validated numerical simulation to determine the thermal-hydraulic boundary conditions has been carried out. Through a saturation-ratio map, the potential for nucleation at different locations over the pool reveals large saturation values in the close vicinity of the pool. In other words, most probably all evaporated Na would become particulate near to the pool surface. At this point, the major influence of the saturation pressures of oxide vapours underline the need for having sound data on this variable for these compounds.

The particle formation process includes homogeneous and heterogeneous nucleation. The homogeneous nucleation has been treated by an approach based on classical nucleation theory. This choice is supported by the higher complexity of other theories (involving additional uncertain parameters), the inherent uncertainty coming from the lack of information on sodium-oxides properties and the huge sensitivity of any homogeneous nucleation theory to variations in boundary conditions (i.e., temperature). As the prevailing conditions for heterogeneous nucleation fall into the kinetic regime, the growth mechanism of condensation on existing particles has been formulated using kinetic theory. As homogeneous nucleation and condensation are simultaneous and competitive processes, two models of particle generation have been assessed. As a result, all the generated oxides during the sodium oxidation are transformed into particle form in a short period of time (10^{-7} s) and homogeneous nucleation can be neglected beyond the first burst of primary particles (the single-burst approach).

The PG model predictions have been analysed for a generic sodium-pool scenario. As expected, large saturation values are found throughout the spatial domain explored which result in very high particle concentrations just above the sodium pool. Thus, in lumped parameter codes, pools should be seen as aerosol generators where the generation rate depends on vaporization rate and nuclei size is to be estimated from nucleation rate theories. This could be seen as a useful input to describe what happens next, i.e., the fractal agglomeration of the particles.

With the aim of implementing the PG model in a lumped parameter code, a methodology to accommodate the 3-D PG model to application in a zero-dimension situation will be the next step of this work. The final outcome will be simple correlations easily implementable for the particle generation rate and the primary particle size.

Acknowledgments

The authors wish to thank the funding received from the 7th Framework Programme of the European Commission via the JASMIN project (contract number 295803). The authors also acknowledge the valuable discussions with Professor Ian Ford (University College London).

References

Andersson, B., Andersson, R., Hakansson, L., Mortensen, M., Sudiyo, R., van Wachem, B., 2012. Computational Fluid Dynamics for Engineers. Cambridge University Press. ISBN 978-1-107-01895-2.

ANSYS Inc., 2008. FLUENT Computational Fluid Dynamics Software, FLUENT User's Guide.

Baskaran, R., Subramanian, V., Venkatram, B., Chellapandi, P., 2011. Sodium aerosol studies for fast reactor safety. Energy Proc. 7, 660–665.

Becker, R., Döring, W., 1935. Kinetische Behandlung der Keimbildung in übersättigten Dämpfern. Ann. Phys. (Leipzig) 24, 719–752.

Beiriger, P., Hopenfeld, J., Silberberg, M., Johnson, R.P., Baurmash, L., Koontz, R.L., 1973. SOFIRE-II User Report. Atomics International AEC-13055, March 1973.

Bergman, T.L., Lavine, A.S., Incropera, F.P., Dewitt, D.P., 2011. Introduction to Heat Transfer. John Wiley & Sons Inc.. ISBN 13 978-0470-50196-2.

CEA, 2015. The ASTRID Project: advanced sodium technological reactor for industrial demonstration. In: 48th Meeting of the Technical Working Group on Fast Reactors, 25–29 May 2015, IAEA, <https://www.iaea.org/NuclearPower/Meetings/2015/2015-05-25-05-29-NPTDS.html>.

Cherdron, W., Jordan, S., 1980. Determination of sodium fire aerosol process coefficients from FAUNA-experiments. In: Proceedings of CSNI Specialists Meeting on Nuclear Aerosols in Reactor Safety, CSNI-45.

Cherdron, W., Jordan, S., 1983. Die Natrium-Brandversuche in der FAUNA-Anlage auf Brandflächen bis 12 m2. KfK 3041.

Cherdron, W., Bunz, H., Jordan, S., 1985. Properties of sodium fire aerosols and recalculation of their behaviour in closed containments. In: Proceedings of CSNI Specialists Meeting on Nuclear Aerosols in Reactor Safety, Kfk3800, CSNI-95.

Cherdron, W., Jordan, S., Lindner, W., 1990. Die Natriumbrand-Untersuchungen in der FAUNA. Teil 1: Poolbrände und Aerosolverhalten. KfK 4358.

Clement, C.F., Ford, I.J., 1999a. Gas-to-particle conversion in the atmosphere: I. Evidence from empirical atmospheric aerosols. Atmos. Environ. 33, 475–487.

Clement, C.F., Ford, I.J., 1999b. Gas-to-particle conversion in the atmosphere: II. Analytical models of nucleation bursts. Atmos. Environ. 33, 489–499.

Dillmann, A., Meier, G.E.A., 1989. Homogeneous nucleation of supersaturated vapors. Chem. Phys. Lett. 160 (1), 71.

Doda, N., Okano, Y., Ninokata, H., 2003. Numerical simulation of sodium pool fire. Nucl. Technol. 144, 175–185.

Farkas, L., 1927. Keimbildungsgeschwindigkeit in Übersättigten Dämpfen. Z. Phys. Chem. (Leipzig) 125, 239.

Fink, J.K., Leibowitz, L., 1995. Thermodynamic and transport properties of sodium liquid and vapor. ANL/RE-95/2.

Fisher, M.E., 1967. The theory of condensation and the critical point. Physics 3, 255.

Ford, I.J., 2004. Statistical mechanics of nucleation: a review. Proc. Inst. Mech. Eng. Part C: J. Mech. Eng. Sci. 218, 883–899.

Ford, I.J., Laaksonen, A., Kulmala, M., 1992. On the Dillmann-Meier theory of nucleation. J. Aerosol Sci. 23 (suppl. 1), 125–128.

Friedlander, S.K., 2000. Smoke, Dust and Haze: Fundamentals of Aerosol Dynamics. Oxford Univ, Press, ISBN 978-0-195-12999-1.

Fuchs, N.A., Sutugin, A.G., 1970. Highly Dispersed Aerosols. Ann Arbor Science Publishing, Michigan.
Garcia, M., Herranz, L.E., Kissane, M., 2014. In-containment nucleation in severe accidents in SFR: Assessment of thermal hydraulic boundary conditions. In: Proceedings of ICAPP 2014, Charlotte, USA, paper 14068.
GIF, 2002. A Technology Roadmap for Generation IV Nuclear Energy Systems. GIF-002-00, U.S. DOE Nuclear Energy Research Advisory Committee and the Generation IV International Forum.
Girault, N., Cloarec, L., Herranz, L.E., Bandini, G., Perez-Martin, S., Ammirabile, L., 2015. On-going activities in the European JASMIN project for the development and validation of ASTEC-Na SFR safety simulation code. In: Proceedings of ICAPP2015, Nice, France, pp. 482–494.
Girshick, S.L., Chiu, C., 1990. Kinetic nucleation theory: a new expression for the rate of homogeneous nucleation from an ideal supersaturated vapor. J. Chem. Phys. 93 (2), 1273–1277.
Hale, B.N., 1986. Application of a scaled homogeneous nucleation-rate formalism to experimental data at T ≪ Tc. Am. Phys. Soc. 33 (6), 4156–4163.
Hilliard, R.K., McCormack, J.D., Hassberger, J.A., Muhlestein, L.D., 1977. Preliminary results of CSTF aerosol behavior test, AB-1. HELD-SA-1381.
Hilliard, R.K., McCormack, J.D., Postma, A.K., 1979. Aerosol behavior during sodium pool fires in a large vessel – CSTF tests AB1 and AB2. HELD-TME 79-28.
Hinds, W.C., 1999. Aerosol Technology: Properties, Behavior, and Measurement of Airborne Particles. Wiley. ISBN: 978-0-471-19410-1.
IAEA, 2006. Fast Reactor Database 2006 Update, IAEA-TECDOC-1531. Vienna.
Jacq, F., 2006. Material data bank interface library. List of materials and properties. ASTEC-V1/DOC/01-14.
Janz, 1988. Thermodynamic and transport properties for molten salts: correlation equations for critically evaluated density, surface tension, electrical conductance, and viscosity data. J. Phys. Chem. Ref. Data 17 (23), 87–149.
Karthikeyan, S., Sundararajan, T., Shet, U.S.P., Selvaraj, P., 2009. Effect of turbulent natural convection on sodium pool combustion in the steam generator building of a fast breeder reactor. Nucl. Eng. Des. 239, 2992–3002.
Kashchiev, D., 2000. Nucleation Basic Theory with Applications. Butterworth-Heinemann. ISBN 0 7506 46829.
Lamoreaux, R.H., Hildenbrand, D.L., 1984. High temperature vaporization behaviour of oxides. I Alkali metal binary oxides. J. Phys. Chem. Ref. Data 13 (1), p151.
Lee, Y.B., Choi, S.K., 1997. A study on the development of advanced model to predict the sodium pool fire. J. Korean Nucl. Soc. 29 (3), 240–250.
Lhiaubet, G., Bunz, H., Kissane, M.P., Seino H., Miyake, O., Himeno, Y., Casselman, C., Such, J.M., Rzekiecki, R., 1990. Comparison of aerosol behaviour codes with experimental results from a sodium fire in a containment. In: International Fast Reactor Safety Meeting, Snowbird, Utah, 12–16 Aug. 1990.
Malet, J.C., Casselman Duverger, C., de Guy, G., Rzekiecki, R., Charpenel, J., 1981. Potential results of spray and pool fires. Nucl. Eng. Des. 68, 195–206.
Malet, J.C., Sophy, Y., Rzekiecki, R., Cucinotta, A., Mosse, D., 1990. Extensive sodium fire studies general survey of the ESMERALDA programme results. In: International Fast Reactor Safety Meeting, Snowbird, Utah, 12–16 Aug. 1990.
Marimuthu, K., 1996. Sodium fire code SFIRE1C for pool fire characteristics. J. Nucl. Sci. Technol. 33 (10), 787–791.
McCormack, J.D., Hilliard, R.K., Postma, A.K., 1978. Recent aerosol tests in the containment systems test facility. HELD-SA-1686.
Menter, F.R., 1994. Two-equation eddy-viscosity turbulence models for engineering applications. AIAA J. 32, 1598–1605.
Miyake, O., Miyahara, S., Ohno, S., Himeno, Y., 1991. Sodium pool combustion codes for evaluation of fast breeder reactor safety. J. Nucl. Sci. Technol. 28 (2), 107–121.
Murata, K.K., Carroll, D.E., Bergeron, K.D., Valdez, G.D., 1993. CONTAIN LMR/1B-Mod. 1, A Computer Code for Containment Analysis of Accidents in Liquid-Metal Cooled Nuclear Reactors. SAND91-1490, Sandia National Laboratories, Albuquerque, New Mexico.
NEA-CSNI, 1979. Nuclear aerosols and reactor safety. A State-of-the Art Report by a group of experts of the NEA Committee on the safety of nuclear installations, June 1979.
NEA, 2009. State-of-the-art report on nuclear aerosols. OECD Nuclear Energy Agency report NEA/CSNI/R(2009) 5.
Newman, R.N., Payne, J.F.B., 1978. The burning rates of sodium pool fires. Combust. Flame 33, 291–297.
Newman, R.N., 1983. The ignition and burning behaviour of sodium metal in air. Prog. Nucl. Energy 12, 119–147.
Oxtoby, D.W., 1998. Nucleation of first-order phase transitions. Acc. Chem. Res. 31 (2), 91–97.
Oxtoby, D.W., Evans, R., 1988. Nonclassical nucleation theory for the gas-liquid transition. J. Chem. Phys. 89 (12), 7521–7530.
Saffman, P.G., Turner, J.S., 1956. On the collision of drops in turbulent clouds. J. Fluid Mech. 1, 16–30.
Sagae, K., Suzuoki, A., 1985. Development of analytical model for sodium pool combustion. J. Nucl. Sci. Technol. 22 (11), 870–880.
Sathiah, P., Roelofs, F., 2014. Numerical modeling of sodium fire – Part II: pool combustion and combined spray and pool combustion Nucl. Eng. Des. 278, 739–752.
Seinfeld, J.H., Pandis, S.N., 2006. Atmospheric Chemistry and Physics: from Air Pollution to Climate Change. Wiley. ISBN: 978-0-471-72018-8.
Senger, B., Schaaf, P., Corti, D.S., Bowles, R., Voegel, J.C., Reiss, H., 1999. A molecular theory of the homogeneous nucleation rate. I. Formulation and fundamental issues. J. Chem. Phys. 110 (13), 6421–6437.
Shaw, G.E., 1989. Production of condensation nuclei in clean air by nucleation of H_2SO_4. Atmos. Environ. 23 (12), 2841–2846.
Shire, P.R., 1977. SPRAY code user's report. HEDL-TME 76-94, Hanford Engineering Development Laboratory, Richland, WA.
SNL, 2015. MELCOR Computer Code Manuals, Vol. 2: Reference Manual. Sandia National Laboratories report SAND2015-6692 R.
Stillinger, F.H., 1963. Rigorous basis of the Frenkel band theory of association equilibrium. J. Chem. Phys. 38, 1486–1494.
Souto, F.J., Haskin, F.E., Kmetyk, L.N., 1994. MELCOR 1.8.2 assessment: Aerosol experiments ABCOVE AB5, AB6, AB7 and LACE LA2. Sandia National Laboratories, SAND94-2116.
Subramanian, V., Baskaran, R., 2007. Initial size distribution of sodium combustion aerosol. Nucl. Technol. 160, 308–313.
Subramanian, V., Sahoo, P., Malathi, N., Ananthanarayanan, R., Baskaran, R., Saha, B., 2009. Studies on chemical speciation of sodium aerosols produced in sodium fire. Nucl. Technol. 165, 257–269.
Takata, T., Yamaguchi, A., Maekawa, I., 2003. Numerical investigation of multi-dimensional characteristics of sodium combustion. Nucl. Eng. Des. 220, 37–50.
Vehkamäki, H., 2006. Classical nucleation theory in Multicomponent systems. Springer-Verlag, Berlin Heidelberg 2006. Printed in Germany. ISBN-10 3-540-29213-6.
Volmer, M., Weber, A., 1926. Keimbildung in übersättigten Gebilden (nucleation of supersaturated structures). Zeitschr. physi. Chemie. 119, 277–301.
Warren, D.R., Seinfeld, J.H., 1984. Prediction of aerosol concentrations resulting from a burst of nucleation. J. Colloid Interface Sci. 105 (1), 136–142.
Yamaguchi, A., Tajima, Y., 2003a. Validation study of computer code SPHINCS for sodium fire safety evaluation of fast reactor. Nucl. Eng. Des. 219, 19–34.
Yamaguchi, A., Tajima, Y., 2003b. Response surface modelling of aerosol release fraction in sodium pool combustion. J. Nucl. Sci. Technol. 10 (40), 862–870.
Yamaguchi, A., Tajima, Y., 2006. A numerical study of radiation heat transfer in sodium pool combustion and response surface modeling of luminous flame emissivity. Nucl. Eng. Des. 236, 1179–1191.
Yamaguchi, A., Tajima, Y., 2009. Sodium pool combustion phenomena under natural convection airflow. Nucl. Eng. Des. 239, 1331–1337.
Zeldovich, J., 1942. Theory of the formation of a new phase, cavitation. Zh. Eksp. Theor. Fiz. 12, 525–538.